Measuring absolute infrared spectral radiance with correlated visible photons: technique verification and measurement uncertainty

Alan Migdall, Raju Datla, Alexander Sergienko, Jeffrey S. Orszak, and Yanhua H. Shih

An experimental system in which correlated photons for radiometric measurements were used has been set up at the National Institute of Standards and Technology. We use visible-IR pairs of correlated photons produced by means of optical parametric downconversion to measure the radiance of a high-temperature IR source at 3.415 and 4.772 μm in an intrinsically absolute manner (i.e., without requiring any externally calibrated radiometric standard). To our knowledge, this is the only radiometric method with which one measures radiance directly, instead of using radiant power and aperture geometry measurements to deduce radiance indirectly. This technique has an additional unusual characteristic: It allows absolute radiometric measurements of IR radiation to be made with high-quality visible detectors. We compare measurements made with this technique with radiance measurements made with conventional means tied to existing radiometric standards. These comparisons show an average agreement to within ~3% between the two methods. The results demonstrate an accuracy consistent with the estimated uncertainty of the current measurements. This is the first time to our knowledge that this method has been used to provide absolute radiance measurements of a source that has been calibrated conventionally, revealing unexpected systematic effects and allowing estimates of the ultimate accuracy of this method. In addition, these measurements are further into the IR than any previous measurements of this process and have produced the highest thermally stimulated downconversion signal yet seen.

OCIS codes: 030.5630, 130.3060, 350.5610.

1. Introduction

Correlated photon techniques have shown promise in two areas of radiometry: absolute measurement of detector quantum efficiency and absolute measurement of source radiance.[1,2] Both of these measurement applications have the unusual characteristics that they are intrinsically absolute in that they do not rely on any externally calibrated radiometric standards, and they allow for IR radiation to be measured with visible detectors. Although several groups have demonstrated the feasibility of these applications[3–10] and the accuracy of the detector efficiency measurement has recently been tested,[11] to the best of our knowledge, no high-accuracy test of the absolute radiance measurement has yet been published. One further characteristic of the radiance technique is that this is the only method that measures radiance directly, i.e., separate radiant power and area measurements are not required. In this study we use the correlated photon technique to measure the radiance of an IR source and compare the results with measurements that we made using conventional means tied to existing radiometric standards. These results allow us to estimate the ultimate accuracy achievable with this method.

2. Theory and Technique Description

With the present method of measuring absolute spectral radiance without externally calibrated standards, one employs the process of optical parametric downconversion (PDC) in which individual photons from a pump beam are converted in a nonlinear crys-

A. Migdall and R. Datla are with the Optical Technology Division, 221/B208, National Institute of Standards and Technology, Gaithersburg, Maryland 20899. When this research was performed, A. Sergienko, J. S. Orszak, Y. H. Shih were with the Department of Physics, University of Maryland Baltimore County, 5401 Wilkens Avenue, Baltimore, Maryland 21228. A. Sergienko is currently with the Department of Electrical and Computer Engineering, Boston University, 44 Cummington Street, Boston, Massachusetts 02215. J. S. Orszak is currently with the American Institute of Physics, One Physics Ellipse, College Park, Maryland 20740.

Received 20 August 1997; revised manuscript received 26 January 1998.

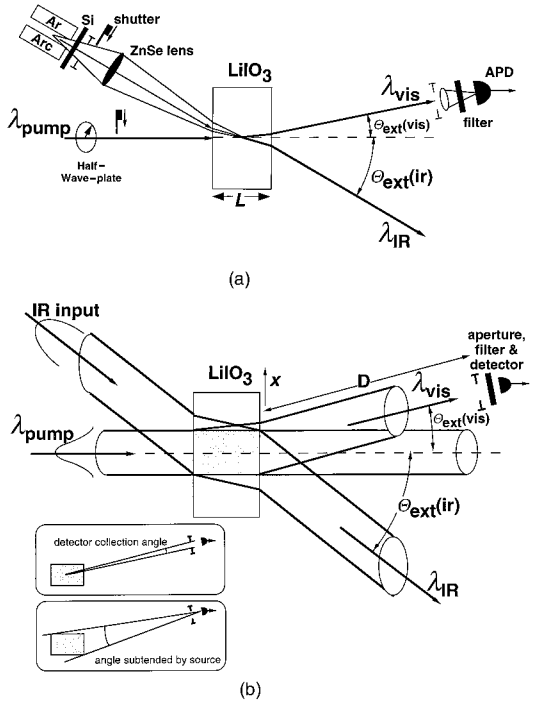

Fig. 1. (a) Scheme for absolute radiance measurement with PDC. (b) Diagram of pump and IR beam interaction region size as viewed from above; x is the horizontal direction across the interaction region at the output face of the crystal.

tal into pairs of photons. The interaction is such that photons from the pump laser beam, in effect, decay into pairs of photons under the restrictions of energy and momentum conservation:

$$\omega_p = \omega_1 + \omega_2, \tag{1}$$

$$\mathbf{k}_p = \mathbf{k}_1 + \mathbf{k}_2, \tag{2}$$

where ω_p and $\mathbf{k}_p$ are frequencies and wave vectors (within the crystal) of the pump, and similarly ω_i and $\mathbf{k}_i$ refer to the downconverted output photons where $i = 1,2$. Since the photons are created in pairs, the detection of one photon indicates with high certainty the existence of the other photon. Because of the energy and the momentum conservation requirements, the direction and the energy of the detected photon can be used to predict not only the existence but also the direction and the energy of the other photon of the pair. It is because this process can be arranged to allow a visible photon to indicate the existence of a second IR photon that it can form the basis of an extremely useful IR radiometry technique.

To measure absolute radiance, a nonlinear crystal pumped by a laser is set up, as described above, to produce correlated IR-visible pairs of photons (Fig. 1). The output of the IR source to be measured is imaged into the crystal so as to overlap the region pumped by the laser and to overlap the output direction of a portion of the downconverted light. The IR beam to be measured must overlap the downconverted output spectrally as well as spatially and directionally. This additional IR input to the crystal enhances the decay of photons from the pump beam into downconverted photons along that overlap direction, however, because these output photons must be produced in pairs, an increase is also seen along the correlated direction. By analogy with an atomic system, this can be thought of as a stimulated decay of pump photons into correlated pairs, whereas the correlated photons produced with only the pump laser for input are the result of spontaneous decay. This spontaneous decay is equivalent to that produced (or stimulated) by a spectral radiance of 1 photon/mode, which can be written as $\mathbf{R}_{\text{vac}} = hc^2/\lambda^5$ (which has the more familiar units of spectral radiance, $\text{W/m}^3\,\text{sr}$).[2] This value can be obtained with the following relationships:

$$L(\lambda) = \frac{c}{4\pi}u, \qquad u = \rho\langle\bar{n}\rangle\frac{hc}{\lambda}, \qquad \rho = \frac{4\pi}{\lambda^4}, \tag{3}$$

where $L(\lambda)$ is the spectral radiance, λ is the wavelength, u is the energy density of a single polarization of a thermal field, ρ is the mode density, $\langle\bar{n}\rangle$ is the average number of photons per mode, c is the speed of light, and h is Planck's constant. Combining these, one gets

$$L(\lambda) = \frac{hc^2}{\lambda^5}\langle\bar{n}\rangle. \tag{4}$$

From this form it is clear that a radiance of 1 photon/mode is hc^2/λ^5.

The quantum field theoretical origin of this 1 photon/mode, which follows the derivation of Louisell *et al.*,[12] is sketched here. The three-wave interaction Hamiltonian, H_I, for the optical parametric process can be written

$$H_I = \tfrac{1}{2}\int \mathrm{d}v\mathbf{P}\cdot\mathbf{E} = \tfrac{1}{2}\int \mathrm{d}v\chi^{(2)}_{ijk}\mathbf{E}_i(r,t)\mathbf{E}_j(r,t)\mathbf{E}_k(r,t), \tag{5}$$

where $\mathbf{P}$ is the nonlinear polarization induced in the medium by the pump electric field $\mathbf{E}$. The polarization is defined in terms of the second-order dielectric susceptibility of the medium, $\chi^{(2)}_{ikj}$, which couples the pump field to the two output fields. The field operators, a_{i0} and $a_{i0}^{\dagger}$, for the creation and the annihilation of photons at the two output frequencies ω_1 and ω_2 can be written as

$$\begin{aligned} a_1(t) &= \exp(-i\omega_1 t)[a_{10}\cosh gt \\ &\quad + i\exp(-i\varphi)a_{20}^{\dagger}\sinh gt], \\ a_2^{\dagger}(t) &= \exp(+i\omega_2 t)[a_{20}^{\dagger}\cosh gt \\ &\quad - i\exp(+i\varphi)a_{10}\sinh gt], \end{aligned} \tag{6}$$

where g is a parametric amplification coefficient proportional to the second-order susceptibility, the crystal length, and the pump field amplitude; a_{i0} and $a_{i0}^{\dagger}$ are the initial operator values; and φ is the phase determined by pump-wave phase.

The average number of photons per mode in the output fields, $n_1(t)$ and $n_2(t)$, is

$$n_1(t) = \langle a_1^\dagger(t) a_1(t) \rangle = n_{10} \cosh^2 gt + (1 + n_{20}) \sinh^2 gt,$$
$$n_2(t) = \langle a_2^\dagger(t) a_2(t) \rangle = n_{20} \cosh^2 gt + (1 + n_{10}) \sinh^2 gt, \quad (7)$$

where n_{10} and n_{20} are the inputs into the $n_1(t)$ and $n_2(t)$ fields, respectively. Since the $\cosh^2 gt$ and $\sinh^2 gt$ factors can be considered constants (which describe the gain in a single pass through the crystal), Eq. (7) can be seen as a two-component gain process with an unusual feature. The 1 in the second term causes there to be a nonzero output, even when both inputs are zero. It is this 1 that can be thought of as the 1 photon/mode stimulating the spontaneous downconversion process. The ratio of the n_1 output with and without an input added to the n_2 channel is just

$$\frac{n_1(\text{on})}{n_1(\text{off})} = \frac{[1 + n_{20}(\text{on})] \sinh^2 gt}{[1 + n_{20}(\text{off})] \sinh^2 gt} = 1 + n_{20}(\text{on}), \quad (8)$$

where $n_{20}(\text{off}) = 0$ and $n_{20}(\text{on}) \neq 0$. (Note in our setup that channel 1 is visible and channel 2 is IR.) This result allows an unknown radiance to be determined in the fundamental units of photons per mode.

To make practical use of these results to measure radiance one must realize several points. First, the radiance [the ratio in Eq. (8) minus one] measured is that which is added to the crystal region being pumped by the laser, so one must account for any input losses. Second, the size of that pumped region is essentially the spatial resolution of the measurement, so one should uniformly bathe that region with the field to be measured to avoid unwanted averaging. Similarly, one must angularly overfill the sensitive region. This angular extent is set with the phase-matching conditions of Eqs. (1) and (2) and the bandwidth of the measurement. These effects are discussed in Section 3, and their sizes are calculated.

3. Experiment

To test the method, we have used the correlated photon technique to measure the radiance of a conventionally calibrated high-temperature Ar-discharge arc source at two IR wavelengths. This is the first time to our knowledge that this method has been used to provide absolute radiance measurements of a source that has been conventionally calibrated, providing a good accuracy test of this method and revealing unexpected systematic effects. In addition, these measurements are further into the IR than any previous measurements of this process and have produced to the best of our knowledge the highest thermally stimulated downconversion signal yet seen.

A. Correlated Photon Measurement of Absolute Radiance: Apparatus

To produce the correlated pairs of photons, we used a linearly polarized Ar^+ laser, power stabilized to 300 mW at 457.9 nm to pump a $LiIO_3$ crystal [Fig. 1(a)]. The crystal, 15 mm × 15 mm by (9.652 ± 0.025) mm long, was mounted in a housing purged with dry air to prevent moisture fogging the surfaces (all ± values in this paper are standard uncertainties). The crystal was cut with its optic axis inclined vertically at 33.6° to the input surface normal. The crystal itself was inclined to the pump direction so that the resulting angle between the optic axis and the pump beam within the crystal was between 28° and 29°. This particular configuration produces correlated visible–IR photon pairs with the visible photons emitted at ~4° and the IR photons emitted at ~25° to 45° from the pump beam direction. (The precise output angles of the correlated photons were obtained with the energy and the momentum constraints,[2,13] the index of refraction data for the crystal,[14] and the orientation of the crystal optic axis with respect to the pump beam.) For our radiance measurements, we selected pairs of photons at two different sets of visible–IR wavelengths, 0.5288 μm/3.415 μm and 0.5065 μm/4.772 μm, where the second wavelength of each pair was the wavelength at which the IR radiance was measured. (We made an initial measurement looking at IR output at 2.25 μm, but it was not pursued owing to a relatively low signal-to-noise ratio at that wavelength.)

In addition to the energy and the momentum requirements discussed above, the polarization of the pump beam must be oriented parallel to the plane defined by the optic axis and the laser direction. This polarization orientation is required by the PDC process defined as Type I, which in our setup uses pump radiation polarized as an extraordinary ray to produce downconverted photon pairs polarized as ordinary rays (perpendicular to the optic axis[13]). A half-wave plate was used to orient the pump beam polarization along the optic axis of the crystal, maximizing the PDC output. Similarly, by rotating the pump beam polarization 90°, one can turn off the PDC production to allow for background subtraction.[15] Shutters in both the pump beam and the IR source beam were also used to look for any nondownconverted light leakage into the detection system.

All detection was done in the visible. An EG&G SPCM-AQ-231 (Ref. 16) actively quenched thermoelectrically cooled Si avalanche photodiode (APD) was used to detect the visible downconverted light. The detector active diameter was 0.26 mm, and the dead time was 68 ns according to a data sheet supplied by the manufacturer. This dead time was used to correct the data, although at the count rates used ($<6000\ s^{-1}$), the correction amounted to less than 0.05%. A 25-mm focal-length lens was placed approximately 25 mm from the APD to concentrate the light. A 0.4-mm-diameter pinhole positioned at the lens and the 560-mm pinhole-to-crystal distance defined the 0.71-mrad detector collection angle [Fig. 1(b)]. A Schott glass GG475 short-wavelength cutoff filter[17] was used to reduce stray pump light on the APD. In addition, two different interference filters centered at (528.8 ± 0.5) nm and (506.5 ± 0.5) nm

(with FWHM passbands of 6 and 3 nm, respectively) were used individually to limit any broadband light on the APD. The peaks of these passbands defined, by means of Eq. (1), the wavelengths of the radiance calibrations to be 3.415 and 4.772 μm, respectively. The APD–filter–lens unit was mounted on an x–y positioning stage to allow its position to be centered on the peak of the downconverted light within the filter passband.

The wall-stabilized Ar arc-discharge source whose spectral radiance was measured is discussed in detail elsewhere and is described just briefly here.[18–20] A discharge is run between two electrodes in a 4.7-mm diameter by a 50-mm-long channel purged with Ar gas. The channel is made from seven stacked insulated plates bored with a single hole in the center of each. Gas ports allow Ar gas to be introduced into the center of the discharge and exhausted at ambient pressure out both ends of the channel and through side ports in some of the channel-defining plates. The discharge was current stabilized at 90.00 A ± 0.01 A with the voltage, ~90 V (producing an equivalent blackbody temperature of from ~4000 to 7000 K in the spectral region of interest). The discharge region, which is viewed end on, emits radiation into a cone somewhat greater than $f/6$, limited by the channel and the discharge region aspect ratios. Because the arc emits prodigious amounts of visible and UV light as well as IR, an antireflection-coated Si substrate was used to limit the arc output to wavelengths longer than 1 μm. A shutter near the imaging lens was used to turn the IR input to the crystal on and off.

The output of the arc was imaged into the crystal with a broadband antireflection (AR)-coated ZnSe lens. A magnification of nearly 2 was used for better overlap of the IR source radiation with the region within the crystal pumped by the laser. For ease of alignment, the arc, its blocking filter, and its imaging lens were mounted on an optical rail with their optic axes aligned to intersect the region of the crystal pumped by the laser. The end of the rail nearest the crystal was held by a two-axis gimbal, so that as the far end of the rail was moved, the optic axis of the source and the imaging system remained centered on the crystal and the pump beam. This arrangement allowed the horizontal and the vertical angular overlap and the focus to be adjusted independently.

B. Correlated Photon Measurement of Absolute Radiance: Measurement Function

To understand these measurements, one must consider two components of the measurement function. First, the IR measurement bandpass is required. One finds this by using Eq. (1) to convert the visible bandpass into the IR region. The second component, affecting the overall efficiency of the measurement, involves how well the IR input beam illuminates the crystal region pumped by the pump laser.

1. *Bandpass*

The bandpass of the IR radiance measurement was defined by the IR wavelengths corresponding to the half-maximum points of the visible bandpass. The visible detection bandwidth itself was determined from the smaller of two limits: a filter limit and a geometric limit. The filter limit, $\Delta\lambda_{vis}$ (filter), is just the bandpass of the visible interference filter in front of the APD. The geometric limit, $\Delta\lambda_{vis}$(geom), is due to the range of downconversion angles seen by the detector and the angle versus the visible wavelength dispersion of the downconverted light, $d\theta(\lambda_{vis})/d\lambda_{vis}$. The range of detected downconversion angles is determined by convoluting the detector collection angle (the angle subtended by the detector as seen from the source) and the angle subtended by the source as seen from the detector [Fig. 1(b)]. This convolution gave nearly the same result as that obtained when just the quadrature sum of the detector and the source angles was taken. In the measurements here, the full-width at half-maximum (FWHM) angle subtended by the source (~1.74 mrad for both measurements) exceeded the detector collection angle (~0.71 mrad, also for both measurements). The effect due to the pump beam divergence was effectively insignificant, because its $1/e^2$ full-angle divergence of 0.36 mrad (=0.21 mrad FWHM) was small relative to both the detector collection angle and the source angular size. Angular spreading due to phase-matching uncertainty was computed to be a very small effect and so was neglected. Note that the geometric considerations discussed here are fundamentally different than those that arise in conventional radiance measurements. In the conventional measurement, the accuracy of the result is directly related to the geometric accuracy, whereas in the correlated measurement, the geometric accuracy affects only the spectral range over which the spectral radiance is determined.

To find the angle subtended by the source, we first determined the apparent size of the PDC source as seen from the detector direction [Fig. 1(b)]. The pump beam at the crystal was assumed to have a transverse Gaussian profile. When viewed from the internal propagation direction of the detected visible light, $\theta_{int}(\lambda_{vis})$, the source column depth profile $I(x)$ is simply

$$I(x) = \int_{x-L\sin\theta_{int}(\lambda_{vis})/2}^{x+L\sin\theta_{int}(\lambda_{vis})/2} \exp(-2x'^2/w_p^2)\mathrm{d}x', \qquad (9)$$

where L is the crystal length, w_p is the $1/e^2$ radius of the pump beam, and x is the horizontal direction across the interaction region at the output face of the crystal. This is just an error function, which for the small angles used here, can be well fit by use of a Gaussian form for determination of a FWHM, I_{FWHM}. The effective angle subtended by the PDC source as seen by the detector is then

$$\Delta\theta_{source}(\lambda_{vis}) = I_{FWHM} * \cos[\theta_{ext}(\lambda_{vis})]/D, \qquad (10)$$

Table 1. Summary of Geometric Bandpass Parameters[a]

λ_{IR} (μm)	λ_{vis} (nm)	$\Delta\lambda_{vis}$(filter) FWHM (nm)	$\Delta\theta_{vis}/\Delta\lambda_{vis}$ (mrad/nm)	$\Delta\lambda_{vis}$(geom) FWHM (nm)	Correlated $\Delta\lambda_{IR}$ FWHM (nm)	$\Delta\theta_{IR}/\Delta\lambda_{IR}$ (mrad/nm)	$\Delta\theta_{IR}$ FWHM (mrad)
3.415	528.8 ± 0.5	6.0 ± 0.5	0.542	3.48	145.0	0.247	35.8
4.772	506.5 ± 0.5	3.0 ± 0.1	0.319	5.95	267.0	0.186	49.6

[a]Angles in the table are all external to the crystal.

where $\theta_{ext}(\lambda_{vis})$ is the visible PDC detection angle external to the crystal and D is the crystal–detector distance. The effective visible bandwidth due to geometric effects is then

$$\Delta\lambda_{vis}(\text{geom}) = \frac{\Delta\theta_{\text{source\&det\&pump}}(\lambda_{vis})}{d\theta_{ext}(\lambda_{vis})/d\lambda_{vis}}, \qquad (11)$$

where $\Delta\theta_{\text{source\&det\&pump}}$ (λ_{vis}) is the FWHM of the convolution (or almost equivalently, the quadrature sum) of the source, the detector, and the pump angles. This convolution resulted in 3.48- and 5.95-nm geometric bandpasses for the (528.8 nm/3.415 μm) and the (506.5 nm/4.772 μm) setups, respectively. For the former measurement, the 3.48-nm geometric bandpass dominated the measurement, because it was smaller than the 6-nm filter bandpass. For the latter case, the 3-nm filter bandpass dominated, because it was smaller than the 5.95-nm geometric bandpass. Table 1 summarizes these results and shows the IR bandpasses correlated to the visible results just calculated.

2. Overlap

Ideally, for the simplest analysis, the pumped region of the crystal should be uniformly illuminated by the IR radiation to be measured. Because of the length of the crystal and the sizes of the pump and the IR beams [Fig. 1(b)], it was not possible to achieve complete uniformity of illumination, so a calculation of the overlap integral was required. (This overlap integral is part of the overall system efficiency discussed later.) To do this integral, the spatial profiles of the IR source and the pump laser were needed. The $1/e^2$ radius of the pump beam was measured to be (0.801 ± 0.015) mm. The profile of the arc was best fit to a parabolic shape with a zero-level cutoff. For comparison purposes, we extracted a $1/e^2$ radius of 4.4 mm (at the crystal position) from this parabolic shape by finding the Gaussian profile with the same half-width as the parabolic shape. The integral of the overlap of the two beams inside the crystal at the particular input angle was ratioed to the integral of the pump shape inside the crystal. The ratios were 0.9460 ± 0.0041 and 0.8576 ± 0.0134 for the 3.415- and the 4.772-μm measurements, respectively, indicating the deviation of this configuration from the ideal of a zero-thickness crystal and adding some to our ultimate uncertainty. We determined the ratio uncertainties by calculating the ratio variation due to the IR beam magnification standard uncertainty, the ±0.5-nm visible wavelength uncertainty, the IR beam width fit uncertainty, the pump beam diameter uncertainty, and the crystal length uncertainty. (These component uncertainties are listed in order of size, with the magnification uncertainty dominating.)

B. Conventional Radiance Measurement

The conventional measurement of the arc spectral radiance was made with an IR spectrometer with an ~20-nm bandwidth and a 77-K HgCdTe photovoltaic detector. This system is described in detail elsewhere.[21] To determine absolute radiance, we swapped the arc and a high-temperature blackbody into and out of the spectrometer input. The spectrometer, its input optics, output optics, and IR detector were all kept fixed as the two sources were exchanged. We determined the temperature of the blackbody by placing a thermocouple into a rear cavity that was integral with the blackbody. The temperature difference between the front and the rear cavities was specified to be less than 0.5 K. The effective emissivity of the blackbody was stated by the manufacturer at 0.999, so its radiance should be well approximated by Planck's law.

4. Results

A. Correlated Method Radiance Determination

From Eq. (8) the absolute radiance of the arc in photons per mode is simply the ratio of the correlated visible signal produced with the arc shutter open to the signal with the arc shutter closed minus one. Because the radiance measured is actually the radiance at the crystal, an additional term is needed to find the radiance of the arc at its origin, a throughput, or total system efficiency factor. The radiance (in photons per mode) of the arc at its origin is then

$$R = \frac{n_{20}(\text{on})}{\varepsilon} = \frac{\dfrac{n_1(\text{on})}{n_1(\text{off})} - 1}{\varepsilon}, \qquad (12)$$

where n_1(on) and n_1(off) are the visible PDC signals with the arc shutter open and closed and ε is the total system efficiency. This efficiency factor contains all systematic effects such as IR beam losses and beam overlap factors [Eq. (9)]. The IR beam loss is the attenuation of the IR signal in its trip from the arc to the center of the crystal, which includes filter, lens, and crystal transmittance losses. The first, the spectral transmittance of the AR-coated Si filter, was

Table 2. Radiance Measurement Method Comparison Results and Uncertainties[a]

	IR Wavelength (μm)			
	3.415		4.772	
	Value	Relative Standard Uncertainty	Value	Relative Standard Uncertainty
IR signal transmittance:				
Si filter transmittance	0.9392	0.0053	0.8444	0.0059
ZnSe lens transmittance	0.9250	0.0054	0.9589	0.0052
$LiIO_3$				
Total external transmittance of half crystal	0.9044	0.0031	0.8503	0.0089
- one surface reflectance	0.0814	0.0002	0.0968	0.0029
- internal transmittance of half crystal	0.9846	0.0031	0.9414	0.0084
Total IR signal transmittance	0.7857	0.0082	0.6885	0.0119
Overlap factor	0.9460	0.0041	0.8576	0.0134
Total system efficiency	**0.7433**	**0.0092**	**0.5905**	**0.0179**
Correlated/spontaneous ratio (measured)	**0.4381**	**0.0072**	**0.9380**	**0.0051**
Radiance by correlated method (ratio/eff) (photon/mode)	**0.5894**	**0.0117**	**1.5886**	**0.0186**
Conventional Radiance measurement convolved with filter bandpass (photon/mode)	**0.6057**	**0.0130**	**1.6455**	**0.0322**
(Conv - Corr)/Conv	**0.027**	**0.018**	**0.035**	**0.037**

[a]The values below each horizontal line indicate the total contribution of the values grouped above the line.

measured with both a prism–grating spectrometer and a Fourier transform infrared (FTIR) spectrometer. The spectral transmittances from each method were then averaged over the IR bandwidths given in Table 1. The results from the two methods were then averaged together. The methods agreed to ±0.5%. An additional measurement of filter transmittance was made at the 3.415-μm wavelength. This was more of an *in situ* measurement, in that the attenuation of the visible downconverted signal was determined from measurements made with the AR-coated Si filter and a bare Si filter placed individually and together in the IR input beam. This measured attenuation and the calculated bare Si attenuation were then used to extract the AR-coated Si filter transmittance at the IR wavelength of 3.415 μm. This value, which was ~2% lower than the spectrometer determined transmittance, was thought to better represent the appropriate transmittance because it gives the transmittance in exactly the same bandwidth as that used for the radiance measurement. This *in situ* measurement was not performed for the 4.772-μm point. These procedures yielded AR-coated Si filter attenuations of 0.9392 ± 0.005 and 0.8444 ± 0.005 at 3.415 and 4.772 μm, respectively.

The transmittance of the ZnSe lens with broad AR coating (3–13 μm) was measured to be 0.925 ± 0.005 at 3.415 μm and 0.959 ± 0.006 at 4.772 μm. We did this by positioning the lens in the output beam of an IR monochromator close enough to a large-area detector so that beam deflection was not a problem. The reflectance of the IR signal at the input surface of the crystal was obtained by use of calculation from the crystal indices, the input angles, and the polarization of the input beam. It must be remembered that although the output of the arc is unpolarized, this downconversion process is sensitive only to light polarized perpendicular to the crystal optic axis. These parameters yielded a calculated reflectance of (8.14 ± 0.02)% and (9.68 ± 0.26)% at 3.415 and 4.772 μm, respectively. We determined the reflectance uncertainties by calculating the reflectance as the IR signal was varied over the $\Delta\theta_{IR}$ FWHM range of angles.

The last component of the attenuation of the optical path is due to absorption of the IR within the crystal itself. The two wavelengths where the radiance measurements were made are, in fact, beyond where the crystal begins to absorb, although they are in two local transmittance maxima. The internal absorptance of the crystal was extracted from FTIR transmittance measurements and reflectance calculations of the $LiIO_3$ crystal. To deal with this absorptance completely rigorously, one should calculate the downconversion process throughout the crystal length as the IR signal is attenuated, but since these absorptances were small [full-length internal crystal absorptances were (2.98 ± 0.6)% and (10.48 ± 1.5)% at 3.415 and 4.772 μm regions, respectively], the absorptance of one half of the crystal length was used as an approximation. Slight adjustments were also made to correct for the fact that the FTIR measurements were made at normal incidence, whereas the radiance measurements were made with the IR beam traversing the crystal at internal angles of 13° and 23°. The final internal transmittances at 3.415 and 4.772 μm were 98.46% and 94.14%, respectively.

The combination of the transmittances of the Si filter, the ZnSe lens, and the $LiIO_3$ crystal gives an overall IR signal transmittance, as seen in Table 2. These transmittances (of 0.7857 and 0.6885) are combined with the overlap factors discussed above to de-

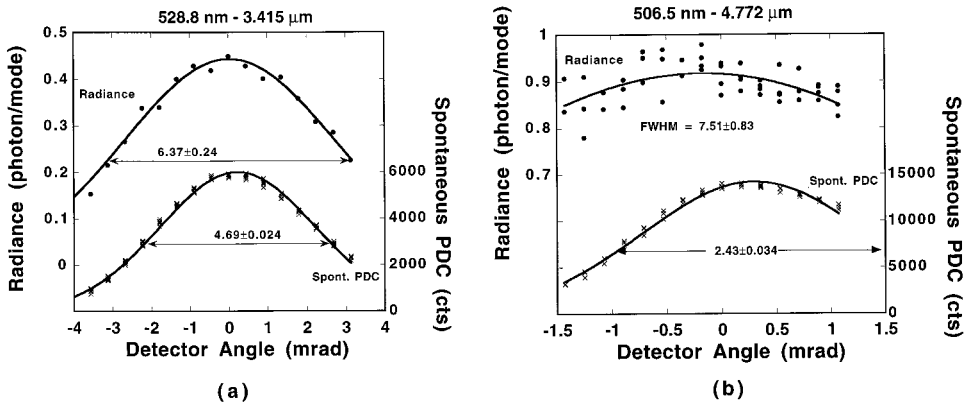

Fig. 2. Spontaneous PDC signal and the ratio of stimulated-to-spontaneous PDC signal versus detection angle for the two pairs of downconverted wavelengths: (a) 528.8 nm to 3.415 μm and (b) 506.5 nm–4.772 μm. (The origin of the angle scale was arbitrarily set near the peak of the signal.) The solid curves are fits to Gaussian profiles with the FWHM indicated.

termine the total system efficiencies of 0.7433 and 0.5905 at 3.415 and 4.772 μm, respectively.

Optical misalignment can have a systematic effect on the measured results, so an alignment procedure was followed to minimize errors. The first step in the optical alignment procedure was to optimize the position and the angle of the APD–filter–lens–pinhole package to maximize the spontaneous downconverted signal. This guaranteed that the detector was looking at the center of the interference filter bandpass. Figure 2 shows the spontaneous downconverted signal and the ratio of stimulated-to-spontaneous signal (or radiance reduced by the system efficiency in units of photons per mode) as the detector package was scanned outward from the pump beam axis (i.e., radially across the spontaneous downconverted output signal). The width of the spontaneous peak is due mainly to the geometric limits [i.e., $\Delta\theta_{\text{source\&det\&pump}}(\lambda_{\text{vis}})$] and to the filter bandwidth that is converted to an angular spread. An estimate of these components summed in quadrature predicted a FWHM of 3.76 mrad (2.13 mrad) at 3.415 μm (4.772 μm) with the detector and the pump angle components contributing the least. These predicted widths average approximately 18% smaller than the measured widths seen in Fig. 2. This result shows that the ADP pinhole diameter was small enough so that spatial variation of the PDC light was slight over the detection aperture, minimizing spatial averaging of the peak.

The overlap integral was calculated as described in Subsection 3.A. The beam overlap itself was optimized with respect to many parameters. The optical rail gimbal mount allowed the horizontal and the vertical angular overlap to be maximized. Slight movement of the x–y position of the imaging lens optimized the translational position of the IR beam with respect to the pump beam inside the crystal. Changing the distance from the crystal to the ZnSe lens and the distance from the lens to the arc allowed the arc image size at the crystal to be varied. These were all adjusted (more or less independently) to maximize the stimulated correlated signal. The maximum corresponded to a 1.97× and a 1.75× magnification of the arc onto the crystal at 3.415 and 4.772 μm, respectively.

After several iterations of these optimizations, a scan of the ratio of the stimulated-to-spontaneous signal was made versus the horizontal detector angle, as shown in Fig. 2. The peak of the curve was fit to a second-order polynomial to extract a maximum value. The maximum ratios, as shown in Table 2, were found to be 0.4381 and 0.9380 for the 3.415- and 4.772-μm measurements, respectively. (The uncertainties are fit parameter standard uncertainties.) Note that these ratios, of order unity, are, to the best of our knowledge, the largest thermally stimulated steady-state downconversion signals ever produced.[9,10] These record values exceed previously published values by more than an order of magnitude. The actual arc radiances are then these ratios divided by the system efficiencies, yielding radiances of 0.5894 ± 0.0117 and 1.5886 ± 0.0186 photon/mode at 3.415 and 4.772 μm, respectively (these are relative standard uncertainties).

B. Conventional Method Radiance Determination

The ratio of the Ar arc output and the blackbody output were measured with collection f-numbers of 12, 18, and 36. These three measurements produced ratios that were identical (to within the noise), indicating that for full angles at least as large as 83 mrad, the arc output was Lambertian. (The aspect ratio of the blackbody cavity was such that its output should be Lambertian over at least an $f/5$ angle.) The result of the conventional measurement of the arc radiance (at $f/12$) in photons per mode, as shown in Fig. 3, was determined from the calculated spectral radiance of the blackbody and the ratio of the arc-to-blackbody signals. A simple ratio was used here because the spectral band of the conventional measurements was much narrower (~20 nm) than the correlated measurement bandwidths. Three such blackbody–arc comparisons were made, one long before the correlated radiance measurements and two shortly after. For the first comparison, the

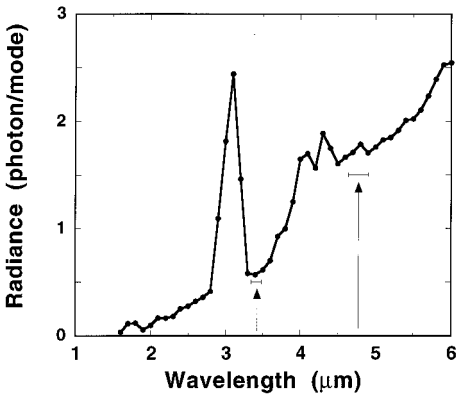

Fig. 3. Conventional measurement of arc radiance converted into units of photons per mode. The arrows indicate the wavelengths at which the two correlated photon radiance measurements were taken. The horizontal lines show the bandpasses (FWHM) of the correlated photon measurements.

blackbody temperature was 1141.4 K ± 1.5 K. For the second and the third comparisons, the blackbody temperature was 1116.2 K ± 1.5 K and 1115.2 K ± 1.5 K, respectively. (The 1.5-K blackbody temperature uncertainty produces a radiance uncertainty of less than 0.0003 photons/mode for wavelengths shorter than 5 μm.) It was though that the fairest determination of the arc radiance would be a straight average of all three measurements, whereas the uncertainty would be taken from the difference between an average of all three measurements and an average of just the two measurements taken last but much closer in time to the correlated measurements. This produced uncertainties of 0.8% and 3.1% for the 3.415- and 4.772-μm regions, respectively.

To determine the total spectral radiance at the wavelengths where the correlated measurements were made, we had to integrate this conventional spectral radiance measurement over the correlated measurement bandpasses. The bandpass used was a Gaussian profile with the centers and the FWHM's chosen to match the correlated measurements. (A Gaussian profile represented the measured filter profile significantly better than a Lorentzian. For the 4.772-μm measurement, the difference between choosing the Gaussian versus a Lorentzian shape resulted in less than 1% difference in the integral. A much greater difference occurred for the 3.415-μm measurement due to a large rise in the IR radiance on one side of the measurement band, which was picked up by the wing of the Lorentzian. We felt justified in using the Gaussian because of its closer approximation to the filter function.) The results of these integrals found the radiances at 3.415 and 4.772 μm to be (0.6057 ± 0.0130) and (1.6455 ± 0.0322) photons/mode, respectively. These are the total relative conventional measurement uncertainties, including the run-to-run variations, the bandwidth convolution just discussed, and a minor component due to the wavelength uncertainty of the conventional IR spectrometer.

C. Comparison of Correlated and Conventional Radiance Measurement Results

As seen in Table 2, the two measurement methods agreed to approximately 3%, which is also the average uncertainty of the comparisons at the two measurement wavelengths. A major source of uncertainty in the comparison was the uncertainty of the conventional measurement. One could certainly reduce this by either monitoring the arc source for variations while making the comparison or by switching to a more stable source. For the correlated measurement, the determination of the system efficiency was the major source of uncertainty. The uncertainty due to the overlap factor could be significantly reduced by use of a shorter crystal is used. This would move the overlap closer to unity, with a commensurate reduction in its uncertainty. Also, moving to a redder pump would reduce the IR beam angles, further improving the overlap. This change might also allow the use of a crystal with transmittance further into the IR, which would reduce the uncertainty. With these improvements, the verification of the correlated photon method could likely be pushed to better than 1% as well as allow measurements to be made beyond 5 μm.

5. Conclusions

These results demonstrate that radiance can be measured in an intrinsically absolute manner by use of correlated photons. The method has two unique advantages: it allows the IR measurement problem to be shifted into the visible where better radiometric detectors are available, and it allows the measurement of spectral radiance directly, without having to measure power and geometric quantities and inferring spectral radiance. This independence of method alone makes the correlated radiance technique a useful addition to radiometry. The accuracy of the method has been initially verified with an average agreement between the correlated and the conventional measurements to ~3%, which is consistent with the average estimated relative standard uncertainty[22] of 3%. There is potential to reduce these uncertainties to 1% or less and to extend the IR spectral range of the technique. This compares favorably with conventional IR spectral radiance measurements that, when they exist, generally do not extend as far into the IR as 5 μm (Ref. 23) or do not significantly surpass 1% uncertainty. These results show that correlated photons can indeed be a useful tool in radiometry and that the method holds enough promise that further studies are warranted.

References and Notes

1. D. N. Klyshko, "Utilization of vacuum fluctuations as an optical brightness standard," Sov. J. Quantum Electron. **7,** 591–594 (1977).
2. D. N. Klyshko, *Photons and Nonlinear Optics* (Gordon & Breach, New York, 1988), p. 325.
3. A. A. Malygin, A. N. Penin, and A. V. Sergienko, "Absolute calibration of the sensitivity of photodetectors using a biphotonic field," Sov. Phys. JETP Lett. **33,** 477–480 (1981).

4. J. G. Rarity, K. D. Ridley, and P. Tapster, "Absolute measurement of detector quantum efficiency using parametric down-conversion," Appl. Opt. **26,** 4616–4619 (1987).
5. S. R. Bowman, Y. H. Shih, and C. O. Alley, "The use of Geiger mode avalanche photodiodes for precise laser ranging at very low light levels: an experimental evaluation," in *Laser Radar Technology and Applications*, J. M. Cruickshank and R. C. Harney, eds., Proc. SPIE **663,** 24–29 (1986).
6. A. N. Penin and A. V. Sergienko, "Absolute standardless calibration of photodetectors based on quantum two-photon fields," Appl. Opt. **30,** 3582–3588 (1991).
7. V. M. Ginzburg, N. G. Keratishvili, E. L. Korzhenevich, G. V. Lunev, A. N. Penin, and V. I. Sapritsky, "Absolute meter of photodetector quantum efficiency based on the parametric down-conversion effect," Opt. Eng. **32,** 2911–2916 (1993).
8. P. G. Kwiat, A. M. Steinberg, R. Y. Chiao, P. H. Eberhard, and M. D. Petroff, "Absolute efficiency and time-response measurement of single-photon detectors," Appl. Opt. **33,** 1844–1853 (1994).
9. A. N. Penin, G. Kh. Kitaeva, and A. V. Sergienko, "Nondestructive measurement of intensity of optical fields using spontaneous parametric down conversion," in *Quantum Electronics and Laser Science*, Vol. 11 of 1991 OSA Technical Digest Series (Optical Society of America, Washington, D.C., 1991), pp. 110–112.
10. G. Kh. Kitaeva, A. N. Penin, V. V. Fadeev, and Yu. A. Yanait, "Measurement of brightness of light fluxes using vacuum fluctuations as a reference," Sov. Phys. Dokl. **24,** 564–566 (1979).
11. A. L. Migdall, R. Datla, A. Sergienko, J. S. Orszak, and Y. H. Shih, "Absolute detector quantum-efficiency measurements using correlated photons," Metrologia **32,** 479–483 (1996).
12. W. H. Louisell, A. Yariv, and A. E. Siegman, "Quantum fluctuations and noise in parametric processes. I," Phys. Rev. **124,** 1646–1654 (1961).
13. J. E. Midwinter and J. Warner, "The effects of phase matching method and of uniaxial crystal symmetry on the polar distribution of second-order non-linear optical polarization," Br. J. Appl. Phys. **16,** 1135–1142 (1965).
14. M. Choy and R. L. Byer, "Accurate second-order susceptibility measurement of visible and infrared nonlinear crystals," Phys. Rev. B **14,** 1693–1706 (1976).
15. Although a small residual signal (which may have been due to imperfect beam polarization or an imperfect crystal) was seen as the waveplate was rotated, it was not of a size to affect the main conclusions of this study. This will be explored further as higher-accuracy comparisons are made.
16. EG&G Optoelectronics, 22001, Dumberry, Vaudreuil (Quebec) Canada J7V 8P7. Certain trade names and company products are mentioned in the text or identified in an illustration to provide an adequate specification of the experimental procedure and the equipment used. In no case does such identification imply recommendation or endorsement by the National Institute of Standards and Technology, nor does it imply that the products are necessarily the best available for the purpose.
17. Schott Glass Technologies Inc. York Ave., Duryea, PA 18642. Certain trade names and company products are mentioned in the text or identified in an illustration to provide an adequate specification of the experimental procedure and the equipment used. In no case does such identification imply recommendation or endorsement by the National Institute of Standards and Technology, nor does it imply that the products are necessarily the best available for the purpose.
18. J. M. Bridges and W. R. Ott, "Vacuum ultraviolet radiometry. 3. the argon mini-arc as a new secondary standard of spectral radiance," Appl. Opt. **16,** 367–376 (1977).
19. J. Z. Klose, J. M. Bridges, and W. R. Ott, "Radiometric calibrations of portable sources in the vacuum ultraviolet," J. Res. Natl. Bur. Stand. **93,** 21–39 (1988).
20. J. M. Bridges and A. L. Migdall, "Characterization of argon arc source in the infrared," Metrologia **32,** 625–628 (1995/96).
21. A. L. Migdall, G. Eppeldauer, and C. Cromer, "Cryogenic optical systems and instruments. VI," J. Heaney and L. Burriesci, eds., Proc. SPIE **2227,** 46–53 (1994).
22. B. N. Taylor and C. E. Kuyatt, "Guidelines for evaluating and expressing the uncertainty of NIST measurement results," NIST Tech. Note 1297 (1994), p. 3.
23. J. Walker, R. D. Saunders, and A. T. Hattenburg, "Spectral radiance calibrations," Natl. Bur. Stands. Special Publication 250-1, 1987 (U.S. Government Printing Office, Washington, D.C., 1987), p. A-4.